

Nonlinear Reconstruction for Liquid-liquid Two-phase Medium Ultrasonic Tomography

Hao Liu, Chao Tan, Feng Dong

Tianjin Key Laboratory of Process Measurement and Control
School of Electrical and Information Engineering, Tianjin University
Tianjin, China
E-mail: fdong@tju.edu.cn

Abstract—Industrial Process Tomography possesses unique advantages in biphasic medium measurement and has received broad attention in the past decades. Aiming at the widely existed low contrast biphasic medium, this paper proposed a nonlinear Ultrasonic Transmission Tomography (UTT). Approach using continuous wave excitation. Considering the refraction effect at the biphasic interface, the reconstruction method with nonlinear forward problem and the improved Simultaneous Algebraic Reconstruction Technique (SART) is proposed with high reconstruction accuracy and reconstruction speed. The performance of the reconstruction is quantitatively compared with the state-of-art reconstruction algorithms, where the proposed method can reconstruct inclusions with their number, size and position clearly identified. Quantitatively, the average Relative Error (RE) is 0.4835 using the proposed method, which is reduced by 49.34% and 40.57% compared with FBP and SART separately. Under parallel computation, the computing time of the proposed method reduced 16.56 times compared with the existing bent-ray tracing method. The proposed image reconstruction algorithm is proved to be an effective and improved approach to the liquid-liquid two-phase flow ultrasonic tomography.

Keywords—Ultrasonic Process Tomography, Low contrast biphasic medium, Continuous-wave excitation, Inverse problem, Ultrasound transmission.

I. INTRODUCTION

Biphasic medium is frequently encountered in the field of process industry, such as the petroleum industry and the chemical engineering industry. Based on medium properties, it can be divided into high contrast biphasic medium (like gas-liquid [1], solid-liquid [2]) and low contrast biphasic medium (like liquid-liquid [3]). Understanding its development mechanism and establishing the computational models require precise measurement of the medium distribution, which is of significance for process monitoring and fault prognosis. Process Tomography (PT) has been developed to conduct visualized measurement of the biphasic medium, and has achieved fruitful development in decades, including the ionizing radiation [4], electrical fields [5][6], laser radiation and Ultrasound [7], Ultrasound can penetrate through the boundary of the testing domain, which can realize non-instructive and non-intrusive

measurement. Accordingly, Ultrasonic Tomography (UT) utilizes the amplitude or time delay information in different projection angles to reconstruction biphasic medium distribution. With the aforementioned advantages, UT is suitable for visualization of industrial process, especially the multiphase medium detection.

Due to the rich information contained in ultrasound waves, UT technique has received growing attention in biphasic medium distribution measurement. Nowadays, the research of UT is continuously moving from offline approaches to online systems and novel sensing strategies, such as multi-wave measurement, fan-beamed transducers and simultaneous excitation. The vast majority of UT researches in industrial applications mainly focus on high contrast biphasic medium, like gas-liquid and solid-liquid medium. However, low contrast biphasic medium also widely exists in various industrial applications. Considering the low acoustic impedance contrast properties of such biphasic medium, the refraction/reflection effect, the scattering effect and the pulse/continuous wave should be taken into consideration when applying the UT methods in measurement.

The above discussion shows the acoustic differences between high contrast and low contrast biphasic medium. Previous studies simplified the UT because many ultrasound effects can be ignored due to high reflection at high contrast interfaces. In low contrast biphasic medium, the core problem is the refraction effect, which is hard to address using conventional method. In this paper, the novel approach of nonlinear low contrast ultrasonic tomography using continuous-wave excitation is proposed to address the attenuation measurement problem and the refraction effect in ultrasound propagation. To describe the direction change in ultrasound propagation, the nonlinear bent-ray tracing is calculated to solve the forward problem, where the concept of “virtual receivers” is proposed to accelerate the calculation. Then, the bent-ray tracing results are formed as the coefficient matrix, which is then used in the inverse problem to reconstruct the attenuation distribution. In the iterations, the “attenuation-to-sound speed” mapping is applied to provide the sound speed information needed in bent-ray tracing. The proposed method is validated numerically with oil bubbles in water to simulate low contrast biphasic medium. The effectiveness of the proposed approach

The authors appreciate the support from the National Natural Science Foundation of China (No. 61571321).

is validated through quantitative and qualitative comparison with state-of-art reconstruction method.

II. SENSOR STRUCTURE AND MEASUREMENT PRINCIPLE

In the testing domain, when the incident ultrasonic wave penetrates through the interfaces between material 1 and material 2, equation (1) estimated the sound pressure change using transmission coefficient T and reflection coefficient R .

$$\begin{cases} T = \frac{4Z_{material1} \cdot Z_{material2}}{(Z_{material1} + Z_{material2})^2} \\ R = \frac{(Z_{material1} - Z_{material2})^2}{(Z_{material1} + Z_{material2})^2} \end{cases} \quad (1)$$

Where Z is the acoustic impedance describing the sound characteristic. Taking the water ($Z_w = 1.494 \times 10^6 \text{ Pa} \cdot \text{s}/\text{m}^3$), oil ($Z_o = 1.079 \times 10^6 \text{ Pa} \cdot \text{s}/\text{m}^3$) and gas ($Z_g = 0.483 \times 10^3 \text{ Pa} \cdot \text{s}/\text{m}^3$) as example, the transmission and reflection coefficient at high contrast interface (gas-water) are 0.0012 and 0.9987, the transmission and reflection coefficient at low contrast interface (oil-water) are 0.9739 and 0.0260. The reflection coefficient at low contrast interfaces is too small with no apparent reflection wave. Therefore, the proposed low contrast ultrasonic tomography approach is operated in transmission mode and the continuous-wave excitation is applied for its higher energy, narrower bandwidth and more centered direction than pulse-wave. It allows higher frequency for bigger attenuation difference between two-phases. Furthermore, the multi-scattering problem is alleviated through continuous-wave excitation.

The measurement principle, as shown in Fig. 1, is to obtain the changing ratio of measurement voltage between background and objective field. To achieve that, a set of transducer array are evenly mounted on the periphery of pipeline. The excitation voltage is added on transducers sequentially until all the transducer have been excited. In data collection, the "one-to-all" strategy is applied resulting in a $m = N \times (N - 1)$ lines of measurements. The inclusion's absorption attenuation coefficient α is defined as follow:

$$\int_{ray} (\alpha_j - \alpha_0) dl = \frac{1}{f_c} \ln \frac{A_s}{A_r} \quad (2)$$

Where A_r and A_s are the receiving signal amplitude with and without inclusions, f_c is the central emitting frequency, α_0 and α_j are the attenuation coefficient of background and at the j th pixel. l is the propagation path length. Simplification s are applied when formulating the equation (2) into linearized model, which is expressed as follow:

$$R \cdot a = \tau \quad (3)$$

Where $a = \alpha_j - \alpha_0$, ($a \in \Omega^{m \times 1}$, $j = 1, \dots, n$) is the relative attenuation coefficient change, $\tau = \frac{1}{f_c} \ln \frac{A_s}{A_r}$, ($\tau \in \Omega^{m \times 1}$) represents the processed measure data, $R = \int_{ray} dl$, ($R \in \Omega^{m \times n}$)

represents the coefficient matrix depicting the geometrical relationship between the i th projection path and j th pixel unit, m represents the amount of projection paths and n represents the pixel unit number. Based on equation (3), the forward problem of continuous-wave UT is to calculate matrix R given the geometrical position relationship and the inverse problem is to calculate a given the pre-calculated R and the measured τ .

III. NONLINEAR IMAGE RECONSTRUCTION ALGORITHM

With the measurement data obtained from transducers, the reconstruction algorithm has to solve the forward problem and the inverse problem to reconstruct the inclusions' distribution in the testing domain. Based on equation (3), the forward problem of continuous-wave UT is to calculate matrix R given the geometrical position relationship, the inverse problem is to calculate a given the pre-calculated R and the measured τ . In the presented work, to address the ultrasound refraction effect, the forward problem is solved by the modified bent-ray tracing (MBR) using the sound speed information, where a simplification is conducted to reduce computing time. The inverse problem is solved by filtered Simultaneous Algebraic Reconstruction Technique (SART) and the attenuation distribution is then obtained. After SART, the sound speed mapping converts attenuation distribution to sound speed distribution, which is needed in the next loop bent-ray tracing.

A. Modified bent-ray tracing forward problem

The ray-based method is widely used for sound speed reconstruction. It addresses the refraction effect (as shown in Fig. 2) through finding propagation rays between each emitter and receiver pair. Neglecting the amplitude variation, it addressed the direction change in refraction effect. Given the sound speed distribution, the propagation ray is traced step by step using Fermat's principle, expressed as follow:

$$\begin{aligned} \vec{r}(s + \Delta s) &= \vec{r}(s) + \frac{d\vec{r}}{ds} \Delta s + \frac{1}{2} \frac{d^2\vec{r}}{ds^2} (\Delta s)^2 + O((\Delta s)^3) \approx \\ \vec{r}(s) + \frac{d\vec{r}}{ds} \Delta s + \frac{1}{2n} \left[\nabla n - \left(\nabla n \cdot \frac{d\vec{r}}{ds} \right) \frac{d\vec{r}}{ds} \right] (\Delta s)^2 \end{aligned} \quad (4)$$

Where n is the refractive index defined by sound speed difference, \vec{r} and s are the position vector and the distance travelled from the emitter, respectively. $\vec{r}(s + \Delta s)$ and $\vec{r}(s)$ indicate the next-step position and the current position respectively. Given the emitter position, the launch angle and the sound speed distribution, the propagation ray can be traced using equation (4). The element s in coefficient matrix R are calculated using the intersecting line segment length of bent-ray and pixel unit.

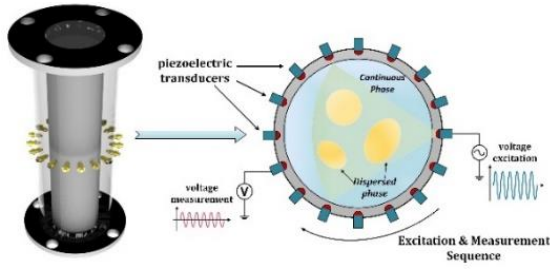


Fig. 1. Measurement principle of transmissive continuous-wave UT

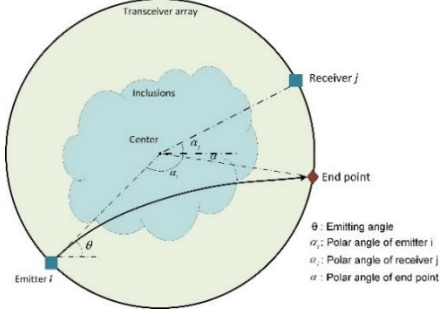


Fig. 2. Schematic diagram of the bent-ray tracing.

Among the information needed in bent-ray tracing, the launch angle is important to the tracing result and has to be pre-determined. Generally, the iterative shooting ray methods are utilized to search optimal launch angle given the emitter and receiver positions. For a specific pair of emitter and receiver, the bent-ray tracing has to be calculated through many loops of shooting ray iteration, which is time-consuming. In this work, we adopted the one-step virtual receiver bent-ray method to increase computing speed. In the method, the launch angle is manually set to be the direction of straight line between emitter and receiver, thus the arrival position after bent-ray tracing is different from actual receiver because of the refraction. A virtual receiver is then placed at the arrival position and the measurement data is updated by the modified measurement data of virtual receiver using linear interpolation. In the proposed modified bent-ray (MBR) forward problem calculation, the input is the sound speed distribution and the transducers' positions. The output is the coefficient matrix R and the updated attenuation measurement data τ .

B. Simultaneous Algebraic Reconstruction Technique

After obtaining the bent-ray coefficient matrix R and the updated measurement data τ , the simultaneous algebraic reconstruction technique (SART) is applied to reconstruct the attenuation distribution, of which the numerical implementation is expressed as:

$$a_j^{(k+1)} = P \left(a_j^{(k)} + \frac{\alpha}{\sum_{i=1}^m r_{ij}} \cdot \sum_{i=1}^m r_{ij} \frac{\left(\tau_i - \sum_{j=1}^n r_{ij} a_j^{(k)} \right)}{\sum_{j=1}^n r_{ij}} \right) \quad (5)$$

Where r_{ij} is the element of matrix R , a_j is the reconstructed attenuation coefficient and τ_i is the i th element of updated measurement data. P is a full-scale two-dimensional Gaussian filter, as expressed below:

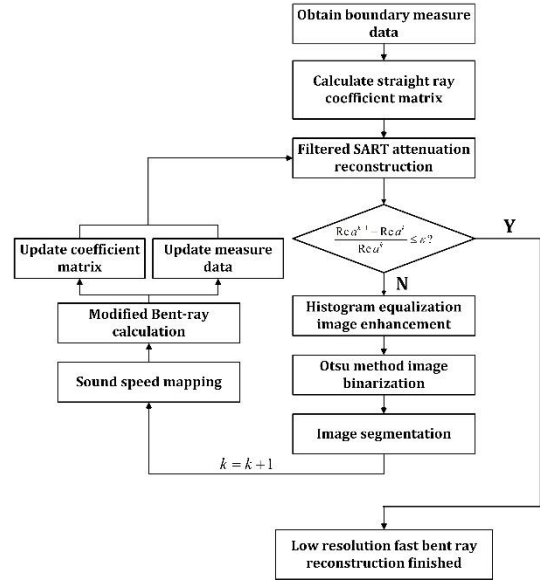


Fig. 3. Overall flowchart of the proposed reconstruction algorithm.

$$P_b = k_r^{-1}(\chi) \int_{-\infty}^{+\infty} \int_{-\infty}^{+\infty} f(\xi) \cdot e^{-\frac{1}{2} \left(\frac{\xi - \chi_b}{\sigma_\xi} \right)^2} d\xi \quad (6)$$

Different from the conventional image filter which calculated the convolution of filter template and image, the proposed Gaussian filter is full-scaled and the filtering process is conducted in every SART iteration. In the filtered SART inverse problem, the input is the modified coefficient matrix R and the updated measurement data τ . The output is the reconstructed attenuation distribution a .

C. Enhancement, segment and sound speed mapping

After the SART reconstruction, the attenuation a is obtained. However, the bent-ray calculation needs sound speed distribution as prior information. Here, we use the “attenuation to sound speed” mapping to connect the attenuation reconstruct result to sound speed distribution, which is managed through image enhancement, segmentation and sound speed mapping.

Once the attenuation image is obtained, the histogram equalization technique is applied to improve image contrast and then the Otsu's method is used for image binarization and inclusion identification. Based on the binary image, the sound speed mapping is conducted, assigning the pre-measured sound speed of dispersed and background medium to the inclusion and the background area separately. Thus, the sound speed distribution is obtained and the “attenuation to sound speed” mapping is finished.

The bent-ray calculation, filtered SART reconstruction and sound speed mapping are iteratively updated as shown in Fig. 3. Firstly, the filtered SART is conducted, resulting in attenuation distribution and then the sound speed mapping changes attenuation distribution to sound speed distribution. The modified bent-ray calculation is then conducted to update coefficient matrix R and measure data τ for SART reconstruction in next loop. The iteration is terminated when the residual of attenuation distribution is smaller than threshold. Because the reconstruction based on bent-ray coefficient matrix

is accurate, the computation generally stops within 5 iterations, therefore the computing speed of iteration is fast.

IV. PERFORMANCE EVALUATION AND RESULTS

To validate the feasibility of the proposed method, a series of simulations are conducted and the reconstruction are compared with the state-of-art SART method in its straight ray approach and the conventional bent-ray approach. The results of the simulative image reconstruction are shown in Fig. 4. The relative error (RE) and correlation coefficient (CC) are defined for evaluating the quality of reconstruction. The derivations are expressed as follow:

$$RE = \frac{\|\sigma - \sigma^*\|_2}{\|\sigma^*\|_2} \quad (7)$$

$$CC = \frac{\sum_{i=1}^I (\sigma_i - \bar{\sigma})(\sigma_i^* - \bar{\sigma}^*)}{\sqrt{\sum_{i=1}^I (\sigma_i - \bar{\sigma})^2 \sum_{i=1}^I (\sigma_i^* - \bar{\sigma}^*)^2}} \quad (8)$$

Where σ is the calculated conductivity and σ^* is the real condition, σ_i and σ_i^* denote the i th pixel unit of σ and σ^* respectively, $\bar{\sigma}$ and $\bar{\sigma}^*$ are the mean values of σ and σ^* . The evaluation results are shown in Table I and the computing time comparison is shown in Table II.

As shown in the figure, the filtered SART in straight rays (SART-SR) has artifacts and shape distortion in reconstruction, which is caused by the linear approximation during the forward problem calculation. The SART-BR method can accurately reconstruct the inclusions number, size and position. The MBR reconstruction is not as accurate as the filtered SART in conventional shooting angle bent-ray calculation (SART-BR). However, as shown in Table II, the MBR method saved the computing time through limited ray tracing number, which is much more faster than the SART-BR. The average traced ray number of SART-BR and MBR are 17888.6 and 992 separately and the average time cost of these two approaches are 6725.59 ms and 445.29 ms.

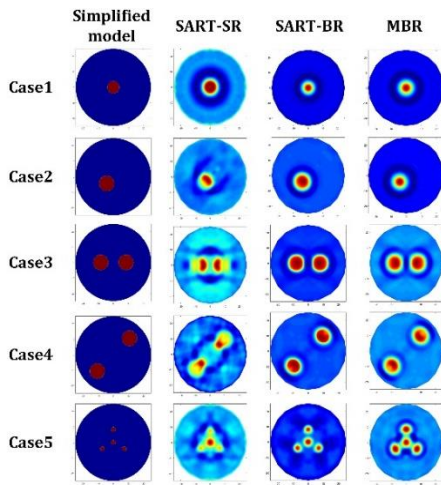


Fig. 4. Simulative image reconstruction results.

TABLE I. QUANTITATIVE ANALYSIS OF RECONSTRUCTION

Model	RE			CC		
	SART-SR	SART-BR	MBR	SART-SR	SART-BR	MBR
case1	0.7724	0.3347	0.3944	0.7619	0.8582	0.8160
case2	0.8015	0.3503	0.4264	0.7025	0.8310	0.8937
case3	0.7314	0.4259	0.4970	0.6987	0.8459	0.8014
case4	0.8942	0.3370	0.3901	0.5696	0.8920	0.8219
case5	0.9295	0.4854	0.5352	0.4592	0.8427	0.7652
average	0.8258	0.3867	0.4486	0.6384	0.8540	0.8049

TABLE II. RAY TRACING NUMBER AND TIME COST EVALUATION

Model	Number of Traced Rays		Time cost (ms)		
	SART-BR	MBR	SART-SR	SART-BR	MBR
case1	15955	992	211.95	6156.25	373.52
case2	16870	992	240.42	6936.72	490.13
case3	19987	992	267.74	7212.90	452.58
case4	18649	992	274.59	6803.31	466.39
case5	17982	992	258.76	6518.75	443.82

V. CONCLUSION

To image the low contrast biphasic medium distribution, the novel approach of nonlinear low contrast ultrasonic tomography using continuous-wave excitation is proposed to address the attenuation measurement problem and the refraction effect in ultrasound propagation while realizing fast computing speed in iterative reconstruction. The benefits of the proposed method in reconstruction accuracy and computing speed are qualitatively and quantitatively validated through simulative measurement data. The future work will focus on dynamic experimental study of low contrast biphasic medium with complicated distribution.

REFERENCES

- [1] C. L. Goh, A. R. Ruzairi, F. R. Hafiz, and Z. C. Tee, "Simulative and experimntal studies: Void fraction detection in a bubble column of a conducting pipe", *IEEE Transactions on Industrial Electronics*, vol. 64, no. 12, pp. 9636-9645, 2017.
- [2] M. Meribout and I. M. Saied, "Real-time two-dimensional imaging of solid contaminants in gas pipelines usign an electrical capacitance tomography system", *IEEE Transactions on Industrial Electronics*, vol. 64, no. 5, pp. 3989-3996, 2017.
- [3] X. Dong, C. Tan, Y. Yuan, and F. Dong, "Measuring oil-water two-phase flow velocity with continuous-wave ultraszxound doppler sensor and drift flux model", *IEEE Transactions on Instrumentation and Measurement*, vol. 65, no. 5, pp. 1098-1107, 2016.
- [4] M. Bieberle, F. Barthel, and U. Hampel, "Ultrafast X-ray computed tomography for the analysis of gassoid fluidized beds", *Chemical Engineering Journal*, vol. 189-190, pp. 356-363, 2012.
- [5] N. Borjindargoon, B. P. Ng, and S. Rahardja, "Music-like algorithm for source localization in electrical impedance tomography", *IEEE Transactions on Industrial Electronics*, vol. 66, no. 6, pp. 4601-4671, 2019.
- [6] C. Tan, S. Lv, F. Dong, and M. Takei, "Imaging reconstruction based on convolutional neural network for electrical resistance tomography", *IEEE Sensor Journal*, vol. 19, no. 1, pp. 196-204, Jan. 2019.
- [7] C. Tan, X. Li, H. Liu and F.Dong, "An Ultrasonic Transmission/Reflection Tomography System for Industrial Multi-phase Flow Imaging", *IEEE Transactions on Indsutrial Electronics Electronics*, DOI: 10.1109/TIE.2019.2891455, 2019.